Orbital angular momentum modes emission from a silicon photonic integrated device for km-scale data-carrying fiber transmission

Liu, Jun; Li, Shimao; Ding, Yunhong; Chen, Shi; Du, Cheng; Mo, Qi; Morioka, Toshio; Yvind, Kresten; Oxenløwe, Leif Katsuo; Yu, Siyuan

Total number of authors:
12

Published in:
Optics Express

Link to article, DOI:
10.1364/OE.26.015471

Publication date:
2018

Document Version
Publisher's PDF, also known as Version of record

Research Article | Vol. 26, No. 12 | 11 Jun 2018 | OPTICS EXPRESS 15471
Optics EXPRESS

Orbital angular momentum modes emission from a silicon photonic integrated device for km-scale data-carrying fiber transmission

JUN LIU,[1,5] SHIMAO LI,[2,5] YUNHONG DING,[3] SHI CHEN,[1] CHENG DU,[4] QI MO,[1,4] TOSHIO MORIOKA,[3] KRESTEN YVIND,[3] LEIF KATSUO OXENLØWE,[3] SIYUAN YU,[2] XINLUN CAI,[2,6] AND JIAN WANG[1,*]

[1]*Wuhan National Laboratory for Optoelectronics, School of Optical and Electronic Information, Huazhong University of Science and Technology, Wuhan 430074, Hubei, China*
[2]*State Key Laboratory of Optoelectronic Materials and Technologies and School of Physics and Engineering, Sun Yatsen University, Guangzhou 510275, China*
[3]*Department of Photonics Engineering, Technical University of Denmark, Kongens Lyngby 2800, Denmark*
[4]*Fiberhome Telecommunication Technologies Co. Ltd, Wuhan 430074, China*
[5]*These authors contributed equally to this work.*
[6]*caixlun5@mail.sysu.edu.cn*
[*]*jwang@hust.edu.cn*

Abstract: We experimentally demonstrate orbital angular momentum (OAM) modes emission from a high emission efficiency OAM emitter for 20-Gbit/s quadrature phase-shift keying (QPSK) carrying data transmission in few-mode fiber (FMF). The device is capable of emitting vector optical vortices carrying well-defined OAM efficiently with the efficiency of the device >37%. Seven modes propagate through a 2-km two-mode and a 3.6-km three-mode FMF with measured optical signal-to-noise ratio (OSNR) penalties less than 4 dB at a bit-error rate (BER) of 2×10^{-3}. The demonstrations with favorable performance pave the way to incorporate silicon photonic integrated devices as transceivers in an OAM-enabled optical fiber communication link.

OCIS codes: (050.4865) Optical vortices; (060.2330) Fiber optics communications; (130.3120) Integrated optics devices.

References and links

1. D. Richardson, J. Fini, and L. Nelson, "Space-division multiplexing in optical fibres," Nat. Photonics **7**(5), 354–362 (2013).
2. P. J. Winzer, "Modulation and multiplexing in optical communication systems," IEEE LEOS Newsletter **23**, 4–10 (2009).
3. J. D. Downie, J. Hurley, J. Cartledge, S. Bickham, and S. Mishra, "112 Gb/s PM-QPSK transmission up to 6000 km with 200 km amplifier spacing and a hybrid fiber span configuration," Opt. Express **19**(26), B96–B101 (2011).
4. D. Sadot, G. Dorman, A. Gorshtein, E. Sonkin, and O. Vidal, "Single channel 112Gbit/sec PAM4 at 56Gbaud with digital signal processing for data centers applications," Opt. Express **23**(2), 991–997 (2015).
5. P. J. Winzer, A. H. Gnauck, C. R. Doerr, M. Magarini, and L. L. Buhl, "Spectrally efficient long-haul optical networking using 112-Gb/s polarization-multiplexed 16-QAM," J. Lightwave Technol. **28**(4), 547–556 (2010).
6. D. Qian, M.-F. Huang, E. Ip, Y.-K. Huang, Y. Shao, J. Hu, and T. Wang, "High capacity/spectral efficiency 101.7-Tb/s WDM transmission using PDM-128QAM-OFDM over 165-km SSMF within C- and L-bands," J. Lightwave Technol. **30**(10), 1540–1548 (2012).
7. T. Richter, E. Palushani, C. Schmidt-Langhorst, R. Ludwig, L. Molle, M. Nölle, and C. Schubert, "Transmission of single-channel 16-QAM data signals at terabaud symbol rates," J. Lightwave Technol. **30**(4), 504–511 (2012).
8. G. Li, N. Bai, N. Zhao, and C. Xia, "Space-division multiplexing: the next frontier in optical communication," Adv. Opt. Photonics **6**(4), 413–487 (2014).
9. R. Ryf, S. Randel, A. H. Gnauck, C. Bolle, A. Sierra, S. Mumtaz, M. Esmaeelpour, E. C. Burrows, R.-J. Essiambre, P. J. Winzer, D. W. Peckham, A. H. McCurdy, and R. Lingle, "Mode-division multiplexing over 96 km of few-mode fiber using coherent 6x6 MIMO processing," J. Lightwave Technol. **30**(4), 521–531 (2012).
10. P. Sillard, M. Bigot-Astruc, and D. Molin, "Few-mode fibers for mode-division-multiplexed systems," J. Lightwave Technol. **32**(16), 2824–2829 (2014).

#319204 https://doi.org/10.1364/OE.26.015471
Journal © 2018 Received 9 Jan 2018; revised 24 Apr 2018; accepted 8 May 2018; published 6 Jun 2018

Optics EXPRESS

11. J. Sakaguchi, Y. Awaji, N. Wada, A. Kanno, T. Kawanishi, T. Hayashi, T. Taru, T. Kobayashi, and M. Watanabe, "Space division multiplexed transmission of 109-Tb/s data signals using homogeneous seven-core fiber," J. Lightwave Technol. **30**(4), 658–665 (2012).
12. B. J. Puttnam, R. Luis, J.-M. Delgado-Mendinueta, J. Sakaguchi, W. Klaus, Y. Awaji, N. Wada, A. Kanno, and T. Kawanishi, "High-capacity self-homodyne PDM-WDM-SDM transmission in a 19-core fiber," Opt. Express **22**(18), 21185–21191 (2014).
13. A. E. Willner, J. Wang, and H. Huang, "Applied physics. A different angle on light communications," Science **337**(6095), 655–656 (2012).
14. A. E. Willner, H. Huang, Y. Yan, Y. Ren, N. Ahmed, G. Xie, C. Bao, L. Li, Y. Cao, Z. Zhao, J. Wang, M. P. J. Lavery, M. Tur, S. Ramachandran, A. F. Molisch, N. Ashrafi, and S. Ashrafi, "Optical communications using orbital angular momentum beams," Adv. Opt. Photonics **7**(1), 66–106 (2015).
15. J. Wang, "Advances in communications using optical vortices," Photon. Res. **4**(5), B14–B28 (2016).
16. J. Wang, "Data information transfer using complex optical fields: a review and perspective," Chin. Opt. Lett. **15**(3), 030005 (2017).
17. J. Wang, J.-Y. Yang, I. M. Fazal, N. Ahmed, Y. Yan, H. Huang, Y. Ren, Y. Yue, S. Dolinar, M. Tur, and A. E. Willner, "Terabit free-space data transmission employing orbital angular momentum multiplexing," Nat. Photonics **6**(7), 488–496 (2012).
18. H. Huang, G. Xie, Y. Yan, N. Ahmed, Y. Ren, Y. Yue, D. Rogawski, M. J. Willner, B. I. Erkmen, K. M. Birnbaum, S. J. Dolinar, M. P. Lavery, M. J. Padgett, M. Tur, and A. E. Willner, "100 Tbit/s free-space data link enabled by three-dimensional multiplexing of orbital angular momentum, polarization, and wavelength," Opt. Lett. **39**(2), 197–200 (2014).
19. J. Du and J. Wang, "High-dimensional structured light coding/decoding for free-space optical communications free of obstructions," Opt. Lett. **40**(21), 4827–4830 (2015).
20. J. Wang, "Metasurfaces enabling structured light manipulation: advances and perspectives," Chin. Opt. Lett. **16**(5), 050006 (2018).
21. Y. Ren, L. Li, Z. Wang, S. M. Kamali, E. Arbabi, A. Arbabi, Z. Zhao, G. Xie, Y. Cao, N. Ahmed, Y. Yan, C. Liu, A. J. Willner, S. Ashrafi, M. Tur, A. Faraon, and A. E. Willner, "Orbital angular momentum-based space division multiplexing for high-capacity underwater optical communications," Sci. Rep. **6**(1), 33306 (2016).
22. Y. Zhao, J. Xu, A. Wang, W. Lv, L. Zhu, S. Li, and J. Wang, "Demonstration of data-carrying orbital angular momentum-based underwater wireless optical multicasting link," Opt. Express **25**(23), 28743–28751 (2017).
23. Y. Zhao, A. Wang, L. Zhu, W. Lv, J. Xu, S. Li, and J. Wang, "Performance evaluation of underwater optical communications using spatial modes subjected to bubbles and obstructions," Opt. Lett. **42**(22), 4699–4702 (2017).
24. A. Wang, L. Zhu, Y. Zhao, S. Li, W. Lv, J. Xu, and J. Wang, "Adaptive water-air-water data information transfer using orbital angular momentum," Opt. Express **26**(7), 8669–8678 (2018).
25. N. Bozinovic, Y. Yue, Y. Ren, M. Tur, P. Kristensen, H. Huang, A. E. Willner, and S. Ramachandran, "Terabit-scale orbital angular momentum mode division multiplexing in fibers," Science **340**(6140), 1545–1548 (2013).
26. A. Wang, L. Zhu, J. Liu, C. Du, Q. Mo, and J. Wang, "Demonstration of hybrid orbital angular momentum multiplexing and time-division multiplexing passive optical network," Opt. Express **23**(23), 29457–29466 (2015).
27. H. Huang, G. Milione, M. P. Lavery, G. Xie, Y. Ren, Y. Cao, N. Ahmed, T. An Nguyen, D. A. Nolan, M.-J. Li, M. Tur, R. R. Alfano, and A. E. Willner, "Mode division multiplexing using an orbital angular momentum mode sorter and MIMO-DSP over a graded-index few-mode optical fibre," Sci. Rep. **5**, 14931 (2015).
28. A. Wang, L. Zhu, S. Chen, C. Du, Q. Mo, and J. Wang, "Characterization of LDPC-coded orbital angular momentum modes transmission and multiplexing over a 50-km fiber," Opt. Express **24**(11), 11716–11726 (2016).
29. S. Chen, J. Liu, Y. Zhao, L. Zhu, A. Wang, S. Li, J. Du, C. Du, Q. Mo, and J. Wang, "Full-duplex bidirectional data transmission link using twisted lights multiplexing over 1.1-km orbital angular momentum fiber," Sci. Rep. **6**(1), 38181 (2016).
30. J. Liu, S. Li, J. Du, C. Klitis, C. Du, Q. Mo, M. Sorel, S. Yu, X. Cai, and J. Wang, "Performance evaluation of analog signal transmission in an integrated optical vortex emitter to 3.6-km few-mode fiber system," Opt. Lett. **41**(9), 1969–1972 (2016).
31. L. Zhu, J. Liu, Q. Mo, C. Du, and J. Wang, "Encoding/decoding using superpositions of spatial modes for image transfer in km-scale few-mode fiber," Opt. Express **24**(15), 16934–16944 (2016).
32. S. Chen and J. Wang, "Characterization of red/green/blue orbital angular momentum modes in conventional G.652 fiber," IEEE J. Quantum Electron. **53**(4), 7200308 (2017).
33. S. Chen and J. Wang, "Theoretical analyses on orbital angular momentum modes in conventional graded-index multimode fibre," Sci. Rep. **7**(1), 3990 (2017).
34. L. Zhu, A. Wang, S. Chen, J. Liu, Q. Mo, C. Du, and J. Wang, "Orbital angular momentum mode groups multiplexing transmission over 2.6-km conventional multi-mode fiber," Opt. Express **25**(21), 25637–25645 (2017).
35. A. Wang, L. Zhu, L. Wang, J. Ai, S. Chen, and J. Wang, "Directly using 8.8-km conventional multi-mode fiber for 6-mode orbital angular momentum multiplexing transmission," Opt. Express **26**(8), 10038–10047 (2018).
36. L. Zhu, A. Wang, S. Chen, J. Liu, and J. Wang, "Orbital angular momentum mode multiplexed transmission in heterogeneous few-mode and multi-mode fiber network," Opt. Lett. **43**(8), 1894–1897 (2018).

Optics EXPRESS

37. L. Zhu, G. Zhu, A. Wang, L. Wang, J. Ai, S. Chen, C. Du, J. Liu, S. Yu, and J. Wang, "18 km low-crosstalk OAM + WDM transmission with 224 individual channels enabled by a ring-core fiber with large high-order mode group separation," Opt. Lett. **43**(8), 1890–1893 (2018).
38. L. Allen, M. W. Beijersbergen, R. J. Spreeuw, and J. P. Woerdman, "Orbital angular momentum of light and the transformation of Laguerre-Gaussian laser modes," Phys. Rev. A **45**(11), 8185–8189 (1992).
39. Y. Ding, C. Peucheret, H. Ou, and K. Yvind, "Fully etched apodized grating coupler on the SOI platform with -0.58 dB coupling efficiency," Opt. Lett. **39**(18), 5348–5350 (2014).
40. S. Li, Y. Ding, X. Guan, H. Tan, Z. Nong, L. Wang, L. Liu, L. Zhou, C. Yang, K. Yvind, L. K. Oxenløwe, S. Yu, and X. Cai, "Compact high-efficiency vortex beam emitter based on a silicon photonics micro-ring," Opt. Lett. **43**(6), 1319–1322 (2018).
41. X. Cai, J. Wang, M. J. Strain, B. Johnson-Morris, J. Zhu, M. Sorel, J. L. O'Brien, M. G. Thompson, and S. Yu, "Integrated compact optical vortex beam emitters," Science **338**(6105), 363–366 (2012).
42. R. Dorn, S. Quabis, and G. Leuchs, "Sharper focus for a radially polarized light beam," Phys. Rev. Lett. **91**(23), 233901 (2003).
43. Z. Bomzon, V. Kleiner, and E. Hasman, "Pancharatnam-Berry phase in space-variant polarization-state manipulations with subwavelength gratings," Opt. Lett. **26**(18), 1424–1426 (2001).
44. A. Niv, G. Biener, V. Kleiner, and E. Hasman, "Manipulation of the Pancharatnam phase in vectorial vortices," Opt. Express **14**(10), 4208–4220 (2006).
45. S. Li, C. Klitis, Z. Nong, S. Gao, M. Sorel, S. Yu, and X. Cai, "Orbital angular momentum mode multiplexer based on multimode micro-ring resonator with angular gratings," in Conference on Lasers and Electro-Optics, OSA Technical Digest (2016) (Optical Society of America, 2016), paper STh3E.5.
46. J. Liu, S. Li, L. Zhu, A. Wang, S. Chen, C. Klitis, C. Du, Q. Mo, M. Sorel, S. Yu, X. Cai, and J. Wang, "Direct fiber vector eigenmode multiplexing transmission seeded by integrated optical vortex emitters," Light Sci. Appl. **7**(3), 17148 (2018).

1. Introduction

The unabated exponential growth of global internet traffic is driving an ever-increasing demand for higher data transmission capacity and more efficient spectral usage in transmission links [1]. To break the coming capacity crunch, a great many of research efforts have been made to investigate different physical properties of a light wave for data transmission, including frequency/wavelength, amplitude, phase, polarization, time. Thus, various advanced multilevel modulation formats and multiplexing techniques, i.e. m-ary quadrature amplitude modulation (m-QAM), orthogonal frequency-division multiplexing (OFDM), wavelength-division multiplexing (WDM), time-division multiplexing (TDM), and polarization-division multiplexing (PDM), have been widely used to increase the transmission capacity [2–7]. Meanwhile, the multiplexing of multiple independent spatial channels, i.e. space-division multiplexing (SDM), has been proposed as a promising technology to boost attractive increase in transmission capacity by exploring the spatial domain of a light wave [1, 8]. There are several different types of orthogonal modal basis sets that are potential candidates for such SDM systems. In fiber optical communications, few-mode fiber (FMF) and multi-core fiber (MCF) are well-known promising candidates enabling efficient SDM [9–12]. In addition to FMF and MCF, another SDM focusing on the spatial phase structure of light beams, known as orbital angular moment (OAM) multiplexing, has also shown its potential use in both free-space, underwater and fiber optical communications to improve the transmission capacity [13–37]. An OAM beam is characterized by a helical phase front of $\exp(il\theta)$ in which l is the topological number and θ refers to the azimuthal angle [38]. Owing to the helical phase structure, an OAM beam features a doughnut intensity profile with a phase singularity at the beam center. The unlimited topological charge values of OAM and the inherent orthogonality between different OAM states facilitate an alternative multiplexing technique, i.e. OAM-division multiplexing.

So far, most of OAM transmission experiments rely on complex and bulky optical components, which are slow to respond, and cumbersome to use [17–29, 31–37]. This severely limits the prospect of its widespread use in future practical systems. In this paper, we experimentally demonstrate a FMF link based on a micro-meter-sized highly efficient silicon integrated optical vortex beam emitter. The device is capable of emitting vector optical vortices carrying well-defined OAM efficiently with the efficiency of the device >37% [39, 40]. Using this device, seven modes, each modulated by 20-Gbit/s quadrature phase-shift

Optics EXPRESS

keying (QPSK) signal have been successfully transmitted through 2-km two-mode FMF (LP_{01} and LP_{11}) and 3.6-km three-mode FMF (LP_{01}, LP_{11} and LP_{21}), respectively.

2. Concept and principle

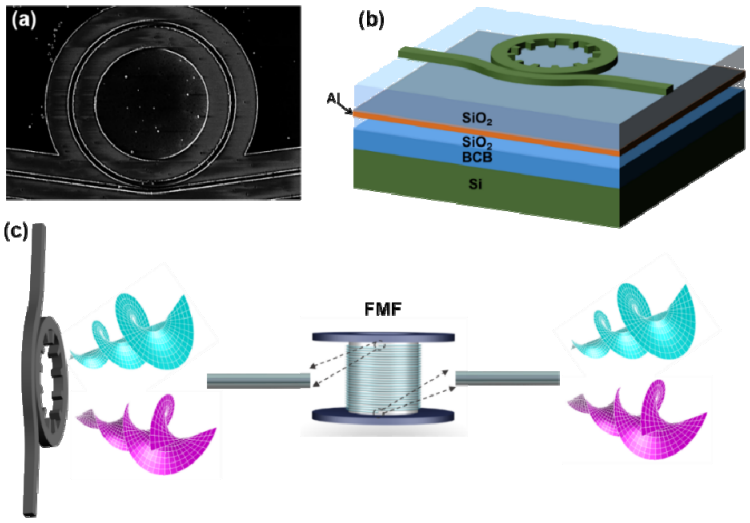

Fig. 1. (a) Measured SEM image of the fabricated device (R = 7.5 μm) with an angular grating patterned along the inner wall of a micro-ring resonator. (b) Schematic illustration of the device with an angular grating patterned along the inner wall of a micro ring resonator and an Al mirror layer. (c) Concept of OAM modes emission from the device for transmission in FMF.

In the silicon integrated optical vortex beam emitter, a micro-ring resonator with angular grating patterned along the inner wall is coupled to an access waveguide for optical input. Figure 1(a) shows the scanning electron microscopy (SEM) image of the fabricated device (R = 7.5 um). The operation principle of this integrated device is to couple the rotating whispering gallery mode (WGM) in the micro-ring resonator to a vertically propagating cylindrical symmetric vector vortex mode. By matching the wavelength of the light with the micro-ring resonance, and by detuning from the grating Bragg wavelength, this device is capable of emitting a propagating field with desired vortex topological charge. The fabricated high emission efficiency OAM emitter is based on substrate transfer technology, and the sketch of the device is depicted in Fig. 1(b). An aluminum mirror is introduced below the micro-ring resonator by wafer bonding technology to the structure to effectively improve the emission efficiency [39, 40].

For the state of polarization (SOP) of the source, since WGMs and the angular grating structure are both cylindrically symmetric, the radiated beams should maintain this symmetry and should be cylindrical vector (CV) beams. In the devices, for quasi-transverse electric (TE) WGMs, the radiated near field is predominantly azimuthally polarized with its Jones vector E_{CV} written as $E_{CV} = \begin{pmatrix} -\sin\theta \\ \cos\theta \end{pmatrix} \exp(il\theta)$. The radiated CV vortex beam can be described as the superposition of two orthogonal scalar vortices, as E_{CV} can be further decomposed into $E_{CV} = \frac{i}{2}\begin{pmatrix} 1 \\ -i \end{pmatrix} \exp i\left[(l+1)\theta\right] - \frac{i}{2}\begin{pmatrix} 1 \\ i \end{pmatrix} \exp i[(l-1)\theta]$, which consists of a right-hand circularly polarized (RHCP) beam with topological charge of $l+1$ and a left-hand circularly polarized (LHCP) beam with $l-1$ [41–44]. The vector beam is emitted into free space and decomposed by a quarter-wave plate (QWP) and a polarizer. After passing through

Optics EXPRESS

the QWP, the LHCP beam and RHCP beam are converted to two orthogonal linearly polarization beams. Then the linearly polarized OAM beam we need is picked out by a polarizer. The linearly polarized beam then couples into and propagates through the FMF, followed by the detection and imaging to form a complete FMF transmission link. The FMF designed to support two modes is 2 km while the other one designed to support three modes is 3.6 km.

3. Experimental setup

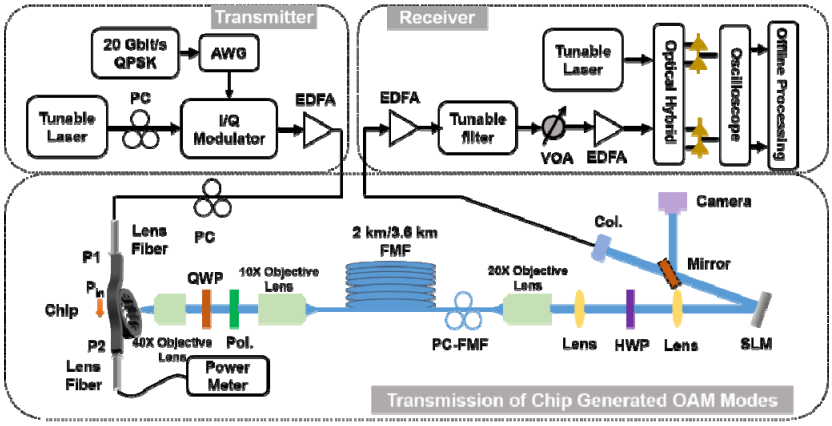

Fig. 2. Experimental setup of OAM modes emission from a silicon photonic integrated device for transmission in FMF. PC: polarization controller. EDFA: erbium-doped fiber amplifier. AWG: arbitrary waveform generator. QWP: quarter-wave plate. Pol.: polarizer. FMF: few mode fiber. PC-FMF: polarization controller on few mode fiber. HWP: half-wave plate. SLM: spatial light modulator. Col.: collimator. VOA: variable optical attenuator.

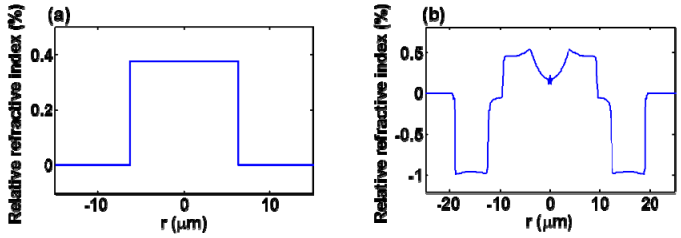

Fig. 3. Relative refractive index profiles of the (a) two-mode and (b) three-mode FMF.

The experimental setup of OAM modes emission from a highly efficient silicon photonic integrated device for transmission in FMF is shown in Fig. 2. At the transmitter side, a 20-Gbit/s QPSK signal is generated by a tunable laser followed by an optical I/Q modulator, which is modulated by an arbitrary waveform generator (AWG). Then the signal is coupled into the input waveguide of the micro-ring resonator. A polarization controller (PC) is used to launch light in the quasi-TE mode in the emitter chip waveguide, and the power is monitored by a power meter placed at the output port of the waveguide. The vortex vector modes with topological charge $l = 1, -1, -2$ are excited when the center wavelength of the tunable laser is 1529.02 nm, 1552.32 nm and 1564.02 nm, respectively. While the vortex mode with topological charge $l = 0$ is splitting to two modes (TM_{01} and TE_{01}) as the strongest cross-coupling occurs at the wavelength of 1538.9 nm and 1541.96 nm respectively due to the second order Bragg reflection. The emitted beam is collimated by a 40X objective lens after emission. Then the collimated circularly polarized beams are converted by a QWP and filtered by a polarizer. The linearly polarized beam is coupled into the FMF by a 10X objective lens. After propagating through the 2 km or 3.6 km FMF, the beam is collimated

Optics EXPRESS

again by another 20X objective lens. The polarization controller (PC) on the FMF (PC-FMF) is adjusted to obtain the OAM states at the FMF output with the smallest possible crosstalk. The SLM is loaded with a reverse phase pattern to convert the OAM mode beam to a Gaussian-like beam which is coupled into a single-mode fiber (SMF) for coherent detection. The half-wave plate (HWP) is used to adjust the polarization of the output light of FMF aligning to polarization of the SLM as the SLM is polarization sensitive. The relative refractive index profiles of two-mode and three-mode FMF are shown in Fig. 3(a) and 3(b), respectively.

4. Experimental results and discussion

First we measure the intensity profiles of the emitted vector vortex modes from a high emission efficiency device with a radius of 7.5. Figures 4(a)-4(f) show the decomposition of the emitted vector vortex mode after the QWP and polarizer, which is scalar vortex mode with topological charge $l = 2$ at the wavelength of 1529.02 nm, $l = 0$ at the wavelength of 1529.02 nm, $l = 0$ at the wavelength of 1552.32 nm, $l = -2$ at the wavelength of 1552.32 nm, $l = 1$ at the wavelength of 1564.02 nm, and $l = -3$ at the wavelength of 1564.02 nm respectively. Figures 4(g)-4(l) display the interference patterns of decomposed linearly polarized beam with a reference Gaussian beam corresponding to the scalar vortex modes above. The polarization of the reference Gaussian beam is –45° or 45° with respect to the fast axis of QWP. In addition, we also measure the intensity distributions of two splitting vector modes with $l = 0$ at the wavelength of 1538.9 nm and 1541.96 nm respectively. Figure 5(a) shows the measured intensity distribution of the TM_{01} mode of the device. Figures 5(b)-5(f) illustrate the measured intensity distributions of TM_{01} mode after a polarizer in the directions indicated by the arrows. The degrees of the polarizer are response to 0, 45, 90, 135 and 180. When the polarizer is rotated, the two-lobe pattern rotates in the same manner, confirming that the radiated beam is with radial polarization. Figure 5(g) shows the measured intensity distribution of the TE_{01} mode of the device. Similar to Figs. 5(b)-5(f), we can confirm that the radiated beam is with azimuthal polarization in Figs. 5(h)-5(l).

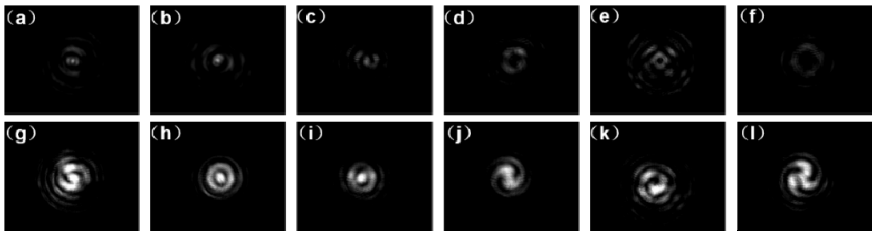

Fig. 4. Measured intensity profiles of the decomposition of the vector vortex modes of a device (R = 7.5 μm) after the QWP and polarizer, (a) $l = 2$ at the wavelength of 1529.02 nm, (b) $l = 0$ atthe wavelength of 1529.02 nm, (c) $l = 0$ at the wavelength of1552.32 nm, (d) $l = -2$ atthe wavelength of 1552.32 nm, (e) $l = 1$ atthe wavelength of 1564.02 nm, (f) $l = -3$ at the wavelength of1564.02 nm respectively.(g)-(l) Measured interference patterns of the decomposition of the vector vortex mode after the QWP and polarizer with a reference Gaussian beam corresponding to the modes above.

Optics EXPRESS

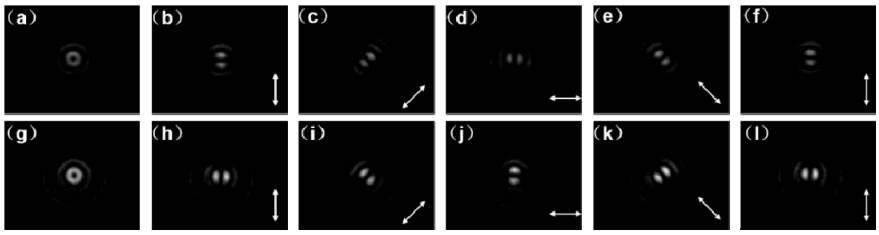

Fig. 5. (a) Measured intensity profile of TM_{01}mode at the wavelength of 1538.9 nm. (b)-(f) Measured intensity profiles of TM_{01} after a polarizer in the directions indicated by the arrows. (g) Measured intensity profile of TE_{01}mode at the wavelength of 1541.96 nm. (h)- (l) Measured intensity profiles of TE_{01} after a polarizer in the directions indicated by the arrows.

Then we measure the radiation spectrum of the high emission efficiency device. Figure 6(a) shows the measured radiation spectrum for the highly efficient device with a radius of 7.5 μm . Figure 6(b) displays the measured radiation spectrum of the low efficiency device with a radius of 7 μm . The spectra are measured by scanning the tunable laser to different wavelength while the input power maintains 10 dBm. We can see that the radiation power of the high emission device increases about 6 dB compared to the other device.

We further measure the intensity profiles of the modes after propagation in the FMF. First, we measure the intensity profiles of decomposed scalar vortex modes $l = 0$ at the wavelength of 1529.02 nm, $l = 0$ at the wavelength of 1552.32 nm, $l = -1$ at the wavelength of 1564.02 nm and vector modes TM_{01} at the wavelength of 1528.9 nm, TE_{01} at the wavelength of 1541.96 nm after propagating through a 2-km two-mode FMF as shown in Figs. 7(a)-7(c), 7(e) and 7(f) respectively. Figures 7(e) and 7(f) also display the measured intensity distributions of TM_{01} and TE_{01} mode after a polarizer in the directions indicated by the arrows. The degrees of the polarizer are corresponding to 0, 45, 90, and 135 which are similar to the profiles before coupling to the FMF. The demodulated intensity profile of $l = -1$ at the wavelength of 1564.02 nm is illustrated in Fig. 7(d). Meanwhile, in Figs. 8(a) and 8(c), we demonstrate the intensity profiles of decomposed scalar modes $l = 2$ at the wavelength of 1529.02 nm and $l = -2$ at the wavelength of 1552.32 nm after propagation of a 3.6-km three-mode FMF. Figure 8(b) and 8(d) illustrate the intensity profiles of the demodulation of $l = 2$ at the wavelength of 1529.02 nm and $l = -2$ at the wavelength of 1552.32 nm after SLM respectively.

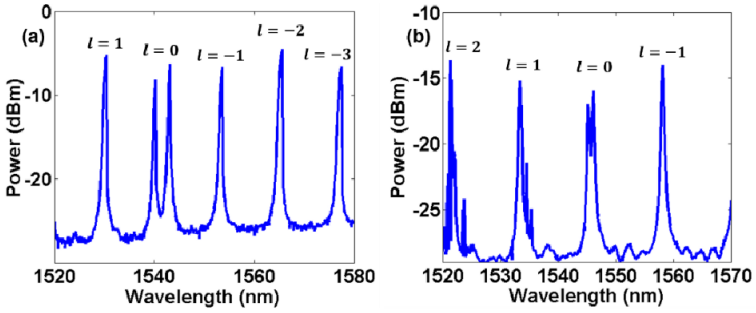

Fig. 6. (a) Measured radiation spectrum of the high emission efficiency device with a radius of 7.5 μm . (b) Measured radiation spectrum of a low efficiency device with a radius of 7 μm .

Optics EXPRESS

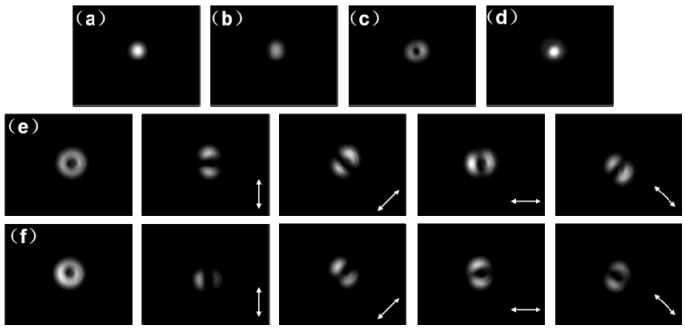

Fig. 7. Measured intensity profiles of (a) $l = 0$ at the wavelength of 1529.02 nm, (b) $l = 0$ at the wavelength of 1552.32 nm, (c) $l = -1$ atthe wavelength of 1564.02 nm after 2 km two-mode FMF respectively, (d) demodulation of $l = -1$ atthe wavelength of 1564.02 nm after SLM, (e) TM_{01} at the wavelength of 1538.9 nm and TM_{01} mode after a polarizer in the directions indicated by the arrows, (f) TE_{01} at the wavelength of 1541.96 nm and TE_{01} mode after a polarizer in the directions indicated by the arrows.

In order to fully investigate the performance of FMF link based on a micro-meter-sized highly efficient silicon integrated optical vortex beam emitter, we further measure the BER performance for all the seven modes with 20-Gbit/s QPSK signal. Figure 9(a) shows the bit-error rate (BER) curves of 2-km two-mode FMF link based on high emission efficiency vortex emitter. Five modes, including decomposed scalar vortex modes $l = 0$ at the wavelength of 1529.02 nm, $l = 0$ at the wavelength of 1552.32 nm, $l = -1$ at the wavelength of 1564.02 nm and vector modes TM_{01} at the wavelength of 1528.9 nm, TE_{01} at the wavelength of 1541.96 nm, propagate through the 2 km two-mode FMF. Meanwhile, BER curves of the decomposed scalar modes $l = 2$ at the wavelength of 1529.02 nm and $l = -2$ at the wavelength of 1552.32 nm propagating through the 3.6-km three-mode FMF are shown in Fig. 9(b). The observed optical signal-to-noise ratio (OSNR) penalties are less than 4 dB at a BER of 2×10^{-3} (enhanced forward-error correction (EFEC) threshold). The inserted images display the typical constellations corresponding to Figs. 9(a) and 9(b).

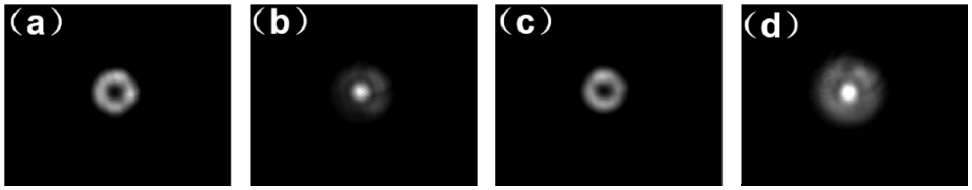

Fig. 8. Measured (a) intensity profiles of $l = 2$ at the wavelength of 1529.02 nm after 3.6 km FMF, (b) intensity profiles of the demodulation of $l = 2$ after a SLM, (c)intensity profiles of $l = -2$ at the wavelength of 1552.32 nm after 3.6 km FMF, (d) intensity profiles of the demodulation of $l = -2$ after a SLM.

Optics EXPRESS

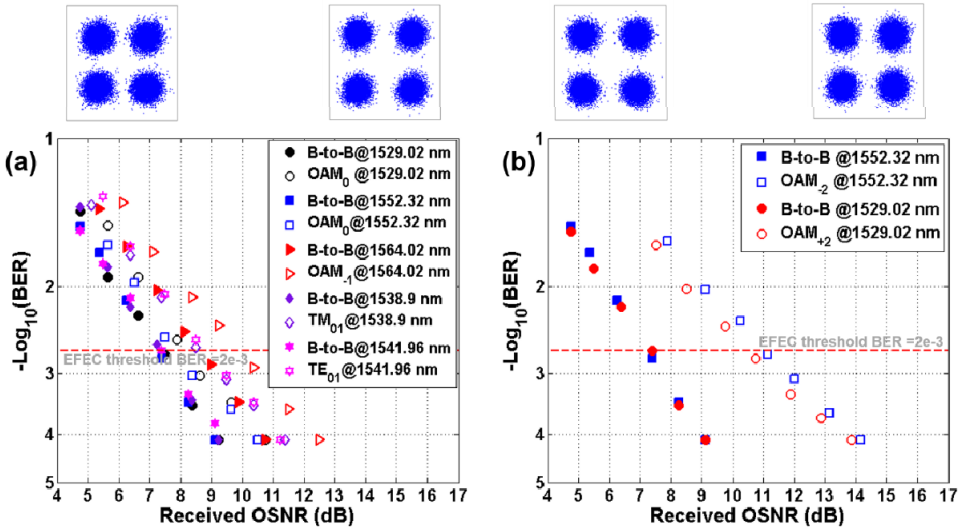

Fig. 9. Measured BER versus OSNR of (a) 2 km two-mode FMF link (b) three-mode FMF link based on a micro-meter-sized highly efficient silicon integrated optical vortex beam emitter.

Remarkably, in the proof-of-concept experiments, the designed and fabricated silicon integrated optical vortex beam emitter generates different OAM modes at different wavelengths. With future improvement, in order to further realize OAM mode multiplexing transmission, different OAM modes at the same wavelength are highly desired. Fortunately, such OAM mode multiplexer can be implemented based on a multimode microring resonator with angular grating [45]. Moreover, we can also use different emitters to generate different OAM modes at the same wavelength by thermally tuning their radiation wavelengths [46].

5. Conclusion

In summary, we experimentally demonstrate a FMF link based on a micro-meter-sized highly efficient silicon integrated optical vortex beam emitter. The device is capable of efficiently emitting vector optical vortices carrying well-defined OAM (efficiency>37%). Using this device, seven modes, each modulated by 20-Gbit/s QPSK signal have been successfully transmitted through 2-km two-mode FMF and 3.6-km three-mode FMF, respectively. The obtained results indicate impressive emission and transmission performance, which opens a door to further employ silicon photonic integrated devices as transceivers in OAM-based optical fiber communication systems.

Funding

National Basic Research Program of China (973 Program) (2014CB340004, 2014CB340003, 2014CB340001); National Natural Science Foundation of China (NSFC) (11574001, 61761130082, 11774116, 11274131); Royal Society-Newton Advanced Fellowship; National Program for Support of Top-notch Young Professionals; Natural Science Foundation of Hubei Province (2018CFA048); Program for HUST Academic Frontier Youth Team; Danish Council for Independent Research (DFF-1337-00152, DFF-1335-00771); Danish National Research Foundation via SPOC (Center for Silicon Photonics for Optical Communications).